Biomaterials 267 (2021) 120484

Contents lists available at ScienceDirect

Biomaterials

journal homepage: www.elsevier.com/locate/biomaterials

Surface Co-presentation of BMP-2 and integrin selective ligands at the nanoscale favors $\alpha_5\beta_1$ integrin-mediated adhesion

Francesca Posa [a], Elisabeth H. Baha-Schwab [a], Qiang Wei [a], Adriana Di Benedetto [b], Stefanie Neubauer [c], Florian Reichart [c], Horst Kessler [c], Joachim P. Spatz [a], Corinne Albiges-Rizo [d], Giorgio Mori [b,**], Elisabetta Ada Cavalcanti-Adam [a,*]

[a] Max Planck Institute for Medical Research, Department of Cellular Biophysics, Jahnstraße 29, Heidelberg, 69120, Germany
[b] University of Foggia, Department of Clinical and Experimental Medicine, viale Pinto 1, Foggia, 71122, Italy
[c] Institute for Advanced Study and Center of Integrated Protein Science (CIPSM), Department of Chemistry, Technische Universität München, Lichtenbergstraße 4, Garching, 85748, Germany
[d] Institut Albert Bonniot, Université Joseph Fourier, INSERM U823, CNRS ERL 5284, Grenoble Alpessite Santé, Grenoble Cedex, 09, F38042, France

ARTICLE INFO

Keywords:
BMP-2
Integrins
Focal adhesions
Surface functionalization
Click chemistry

ABSTRACT

Here we present the use of surface nanopatterning of covalently immobilized BMP-2 and integrin selective ligands to determine the specificity of their interactions in regulating cell adhesion and focal adhesion assembly. Gold nanoparticle arrays carrying single BMP-2 dimers are prepared by block-copolymer micellar nanolithography and azide-functionalized integrin ligands (cyclic-RGD peptides or $\alpha_5\beta_1$ integrin peptidomimetics) are immobilized on the surrounding polyethylene glycol alkyne by click chemistry. Compared to BMP-2 added to the media, surface immobilized BMP-2 (iBMP-2) favors the spatial segregation of adhesion clusters and enhances focal adhesion (FA) size in cells adhering to $\alpha_5\beta_1$ integrin selective ligands. Moreover, iBMP-2 copresented with $\alpha_5\beta_1$ integrin ligands induces the recruitment of $\alpha_v\beta_3$ integrins in FAs. When copresented with RGD, iBMP-2 induces the assembly of a higher number of FAs, which are not affected by $\alpha_5\beta_1$ integrin blocking. Our dual-functionalized platforms offer the possibility to study the crosstalk between integrins and BMP receptors, and more in general they could be used to address the spatial regulation of growth factors and adhesion receptors crosstalk on biomimetic surfaces.

1. Introduction

In mesenchymal tissues, the extracellular matrix (ECM) is a complex three-dimensional network consisting of several proteins and glycosaminoglycans. The ECM not only supports cells by providing an appropriate scaffold fundamental for the maintenance of tissue architecture, but also modulates many different processes such as cell spreading, growth, migration and differentiation [1–4]. Besides binding to each other, ECM glycoproteins also present domains for the binding and release of growth factors (GFs), representing a platform for the control of GF local concentration and signaling [5]. These complex interactions between different molecular components of the ECM are further responsible for the physico-chemical guidance of cell responses, mainly mediated by receptors present at the cell membrane. How the interactions between ECM proteins and GFs are locally regulated and participate to adhesion remains largely unexplored, due to the limited availability of *in vitro* systems that allow to analyze these aspects at the nanoscale level.

Cell adhesion to the ECM is mainly mediated by integrins, heterodimeric transmembrane receptors which, once activated by the presence of ECM ligands, form clusters. Integrins connect the ECM compartment with the actin cytoskeleton by recruiting several intracellular molecules, giving rise to the formation of anchoring structures: the focal adhesions (FAs) [6–9]. The β subunit of integrins has a crucial role for the connection and regulation of cytoskeleton during cell adhesion and migration [10]. Integrin-mediated adhesions establish the mechanical anchoring of cells to the ECM and transmit crucial signals inside the cell to regulate survival, proliferation and differentiation [11–15]. Integrin activation and downstream signaling is further strengthened by the interaction with other cell surface receptors, e.g. GF receptors [16]. The

* Corresponding author.
** Corresponding author.
E-mail address: eacavalcanti@mr.mpg.de (E.A. Cavalcanti-Adam).

https://doi.org/10.1016/j.biomaterials.2020.120484
Received 5 May 2020; Received in revised form 14 October 2020; Accepted 21 October 2020
Available online 26 October 2020

bidirectional crosstalk between integrins and GF receptors is taking place at different levels and a robust synergy between receptor tyrosine kinases and integrins, involving specific integrin subunits, has been identified and characterized in several studies [17–20]. In this scenario, an emerging role has been attributed to the serine/threonine kinases family of receptors. GFs also modulate the interaction between integrins and ECM glycoproteins in the guidance of tissue healing and regeneration processes. This aspect becomes particularly important in therapeutic approaches, e.g. based on metal prothesis replacement or scaffold engraftment, where GFs such as Bone morphogenetic protein-2 (BMP-2) are frequently used [21,22].

BMP-2 belongs to the transforming growth factor-β (TGF-β) superfamily and exerts its function by binding to serine/threonine kinases receptors, BMPRs (BMPR type I and BMPR type II). Upon binding of BMP-2, the activation of the BMPRs takes place, leading to both Smad-dependent and Smad-independent BMP-signaling pathways [23]. The flexibility of BMP-2 signaling implies that the induction of a specific pathway is determined by receptor availability, spatial organization and association in complexes on the cell membrane [24,25]. Over the last two decades, a growing body of research has shown that BMP-2 impacts actin cytoskeleton organization and plays a role in cell adhesion and migration [19,26–28] through integrin/BMPR crosstalk.

Although *in vitro* studies on cell adhesion have mainly focused on the use of recombinant human BMP-2 (rhBMP-2) added in solution, matrix-bound approaches were recently developed to reduce the GF concentrations used and to enhance GF biological activity [29]. These approaches are inspired by the ability of BMP-2 to interact with matrix molecules, such as fibronectin, which present integrin binding sites. In this way, the localized and spatial regulation of integrin/BMPR crosstalk might be favored. The Picart lab has developed a polyelectrolyte layer-by-layer approach to present matrix-bound BMP-2 [20]. Furthermore, using these platforms, Fourel et al. [19] showed the mutual regulation of BMP- and integrin-mediated signaling: only when presented in matrix-bound form, BMP-2 induces adhesion formation in cells on soft matrices, overriding impaired cell adhesion mechanics. In turn, $\alpha_v\beta_3$ integrin binding to fibronectin produced by the cells, is not only crucial for spreading, but also for BMP-dependent Smad signaling. This finding is in contrast with what has been previously reported by Martino M et al. [30], on the synergy of $\alpha_5\beta_1$ integrins with GFs, due to the proximity of the respective binding sites in engineered fibronectin domains. Although it is difficult to identify which integrin is involved in the adhesion crosstalk with BMP-2 because these two systems are so different, it still emerges that matrix-bound BMP-2 is more effective than the soluble one.

In designing materials for the presentation of matrix-bound BMP-2, which allows the study of BMP-integrin crosstalk for cell adhesion, a current challenge is to achieve a spatial control over the presentation of integrin ligands and BMP-2 molecules to cells, while keeping physical proximity of the two activated receptors. So far the copresentation of BMP-2 and adhesive ligands has been achieved through micropatterning approaches [31]. We have previously shown that the covalent binding of rhBMP-2 to a self-assembled monolayer, consisting of an heterobifunctional linker which addresses its free amine residues, maintains the GF bioactivity [32] and still triggers Smad signaling pathway even when used at very low amounts [33]. We have also designed a platform presenting immobilized integrin selective ligands to bind and activate $\alpha_5\beta_1$ and $\alpha_v\beta_3$ integrins to control cell spreading and assembly of integrin-mediated focal adhesions [34]. These integrin ligands are peptidomimetic compounds which are highly-selective for specific integrins and determine cell adhesion and focal adhesion assembly [35,36]. In the present study, we combine these two approaches to achieve specificity and spatial control over the co-presentation of BMP-2 and selective integrin ligands. Since our purpose is to discriminate the specific contribution of $\alpha_5\beta_1$ or $\alpha_v\beta_3$ integrins, we probe this aspect by respecting the space between integrin ligands required to form adhesion sites [37]. With this setup, we control GF surface density at the nanoscale while achieving cell adhesion mediated by the specific integrin types, and we investigate early cell adhesion and spreading regulated by BMP-2.

2. Results and discussion

To determine (i) if surface immobilized BMP-2 (iBMP-2) at the nanoscale influences cell spreading and focal adhesion assembly, and (ii) whether its effects are specific for the integrin subtype bound to the surface, cells were cultured on dual-functionalized nanopatterned surfaces (Fig. 1) presenting iBMP-2 covalently bound to gold nanoparticles with defined spacing, and integrin ligands bound to orthogonally modified polyethylene glycol (PEG) coating carrying alkyne groups. By adapting the dual-functionalized platforms developed by Schenk at al. [38], the integrin ligands were bound to the PEG at a surface density of 0.53 ng/cm^2. As integrin ligands, we used $\alpha_5\beta_1$ integrin selective peptidomimetic antagonists [36] (Fig. S1A) or cRGDfK (indicated as cRGD) ligands (Fig. S1B), which have high affinity for $\alpha_v\beta_3$ integrins. Synthetic integrin selective peptidomimetics bound to substrates have been widely used to study integrin-mediated adhesion taking advantage of their high selectivity and affinity for specific integrins of interest [34,36,39].

We chose a spacing of 50 nm between the single iBMP-2, since we previously showed that this is sufficient for triggering an elevated and prolonged BMP-mediated signaling in C2C12 cells [33]. The amount of BMP-2 corresponds to approximately 1 ng/cm^2, as previously characterized in Schwab EH et al. [33] by quantification of the surface bound molecules using atomic force microscopy. This is significantly less than the lowest amount reported in literature so far (31 ng/cm^2) [40]. Using our chemical immobilization strategy, BMP-2 is covalently bound to a bifunctional linker, immobilized on the surface, avoiding a possible denaturation of the protein which, instead, could occur when a GF is pre-coupled to the linker and immobilized through a single step [41–43]. There are also non-covalent binding approaches and, among them, the biotin-streptavidin system is one of the most commonly used [44]. The lack of site specificity and difficulty in controlling the labeling degree might hinder receptor binding and impair BMP-2 biological activity. Additionally, it does not allow to control the exact number of immobilized molecules, an aspect which some researchers have attempted to overcome through modifications of the protein (expression of his-tag); also in this case a consequent alteration of the biological activity is possible [22]. With our setup, although the molecule orientation cannot be controlled, its amount is finely regulated when combined with surface nanopatterning strategies.

Cell adhesion and spreading kinetics were determined by time-lapse phase contrast microscopy (Fig. 2, and Supplementary Movies 1-6). Over a 4 hr-period, due to the protein repellent properties of the PEG coating, in absence of integrin ligands (negative control) cells did not adhere to the surface, even in presence of BMP-2 (Fig. 2A, panels a–c). When integrin ligands were bound to the surface by click chemistry (Fig. 2A, panels d–i), cell spreading kinetics was different. Interestingly, the spreading area was significantly increased on $\alpha_5\beta_1$ integrin selective ligands combined with iBMP-2 (Fig. 2B upper plot, blue line), whereas addition of the soluble growth factor to the culture media (sBMP-2) did not affect spreading and was comparable to the control in absence of BMP-2 (Fig. 2B upper plot, red and green lines). On cRGD, cell spreading area was slightly reduced in comparison to the one on the $\alpha_5\beta_1$ integrin selective ligands (Fig. 2B lower plot), confirming our previous observations [34] and with no statistically significant differences observed between sBMP-2 and No BMP-2 treatments (Fig. 2B lower plot, red and green lines). Even if the presence of iBMP-2 induced an increase in the projected cell area (Fig. 2B lower plot, blue line), which was statistically significant when compared to sBMP-2 and No BMP-2 treatments, this effect was slower and significantly lower than the one observed with $\alpha_5\beta_1$ integrin selective ligands. Taken together, these results suggest that the proximity of surface bound $\alpha_5\beta_1$ integrins and BMPRs favors early spreading of C2C12 cells on stiff substrates.

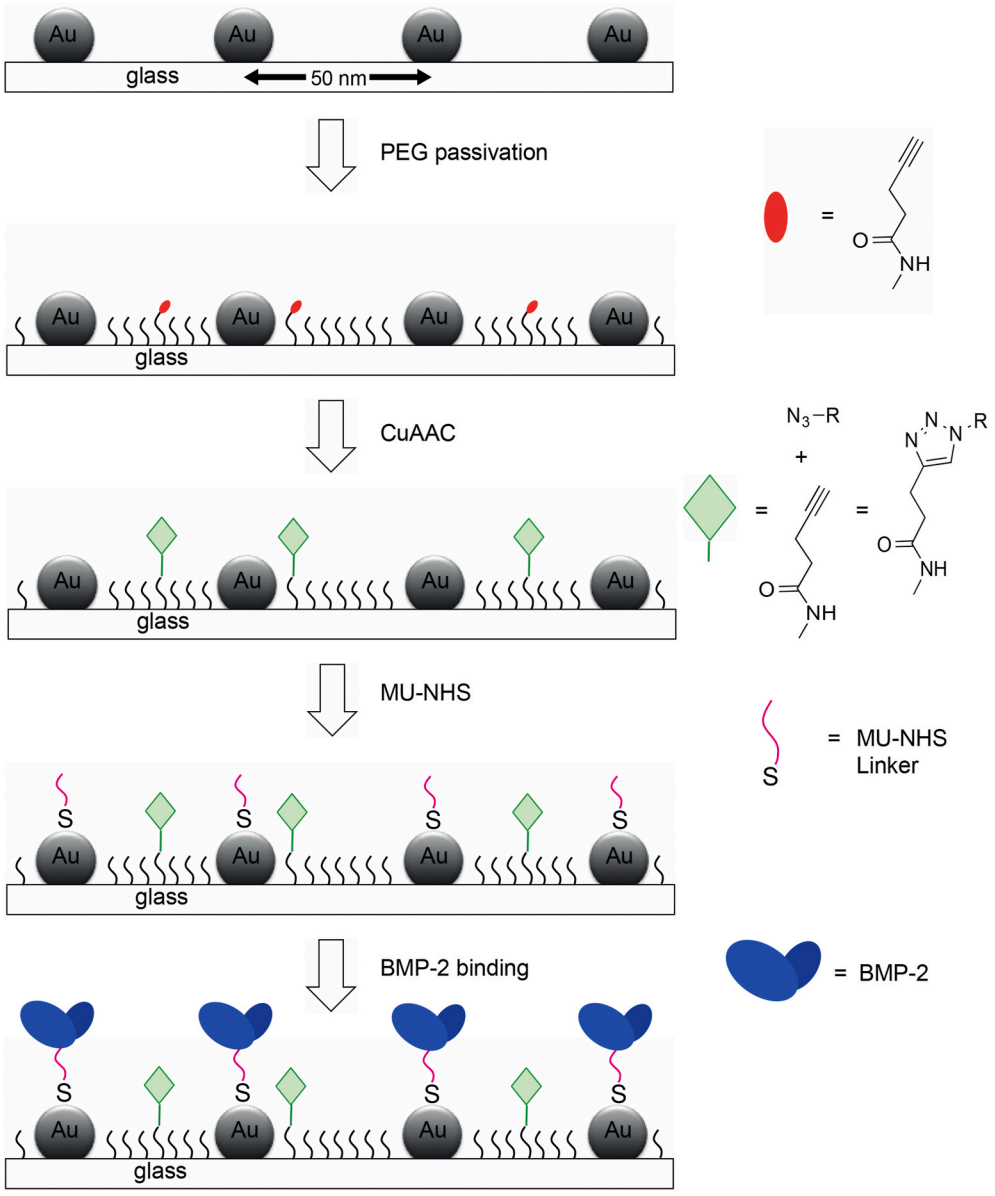

Fig. 1. Experimental set-up for the preparation of nanopatterned surfaces presenting integrin ligands and immobilized BMP-2. Gold nanoparticle arrays, having a 8–10 nm size and placed at an interparticle distance of 50 nm, are produced by BCMN. The space between the nanoparticles is covered with a layer of 99:1 PEG2000 and PEG3000 carrying alkyne end groups (in red). PEG-alkyne are then functionalized with an azide-containing peptide *via* click reaction (in light green). Gold nanoparticles are functionalized with the heterobifunctional linker MU-NHS (magenta line) and subsequently with rhBMP-2 (dimer in blue). (For interpretation of the references to color in this figure legend, the reader is referred to the Web version of this article.)

Supplementary video related to this article can be found at https://doi.org/10.1016/j.biomaterials.2020.120484.

Fourel et al. showed the key role of matrix-bound BMP-2 in the induction of β_3 integrin-dependent cell spreading [19], thus we next evaluated focal adhesion (FA) size and number in C2C12 cells 4 h after seeding on the surfaces. Cells were analyzed for the subcellular distribution of vinculin, a marker of FA formation [45], using indirect immunofluorescence microscopy. Representative cells adhering to the different substrates are shown in Fig. 3.

Since only few cells adhered to surfaces without the integrin ligands and vinculin clusters were hardly detectable (Fig. 3a–c) regardless of the presence of BMP-2, it was not possible to perform FAs image analysis for these samples. For cells adhering to cRGD, the ligand specific for $\alpha_v\beta_3$ integrin (Fig. 3d–f), vinculin clusters were present predominately at the cell periphery in absence of BMP-2, suggesting that FAs are assembled by $\alpha_v\beta_3$ integrin binding (Fig. 3d). The addition of BMP-2 in culture media (Fig. 3e) or the immobilization of BMP-2 onto the surface (Fig. 3f) induced formation of peripheral FAs. Additionally, more central and elongated vinculin-enriched adhesions were observed. When $\alpha_5\beta_1$ integrin selective ligands were immobilized on the surface, all cells displayed vinculin clusters (Fig. 3g–i). However, the distribution of the adhesion sites depended on the mode of presentation of BMP-2. Indeed small punctate vinculin clusters appeared distributed all over the ventral side of cells in absence of BMP-2 (Fig. 3g) or upon BMP-2 addition in solution (Fig. 3h). The presentation of $\alpha_5\beta_1$ integrin selective ligands together with iBMP-2 induced the strengthening of β_1 integrin containing adhesion sites by forming more elongated peripheral vinculin clusters (Fig. 3i).

A quantitative analysis of FAs [46] revealed that the total area covered by FAs for each cell was significantly greater for cells adhering to substrates presenting iBMP-2 functionalized with either cRGD or $\alpha_5\beta_1$ integrin selective ligand, in comparison to the samples without the growth factor or with sBMP-2 (Fig. 3j). Nevertheless, a low number of FAs per cell was observed only for cells adhering to surfaces with $\alpha_5\beta_1$ ligand and iBMP-2 (Fig. 3k), supporting the conclusion that vinculin was organized in large clusters, resembling more mature FAs. This was also confirmed by the analysis of FA length (Fig. 3l), which was higher for cells on the surfaces presenting $\alpha_5\beta_1$ integrin ligands compared to cRGD functionalized surfaces. Thus, the ligand type impacts FA number and size: the number is increased when $\alpha_v\beta_3$ integrin can also bind to the

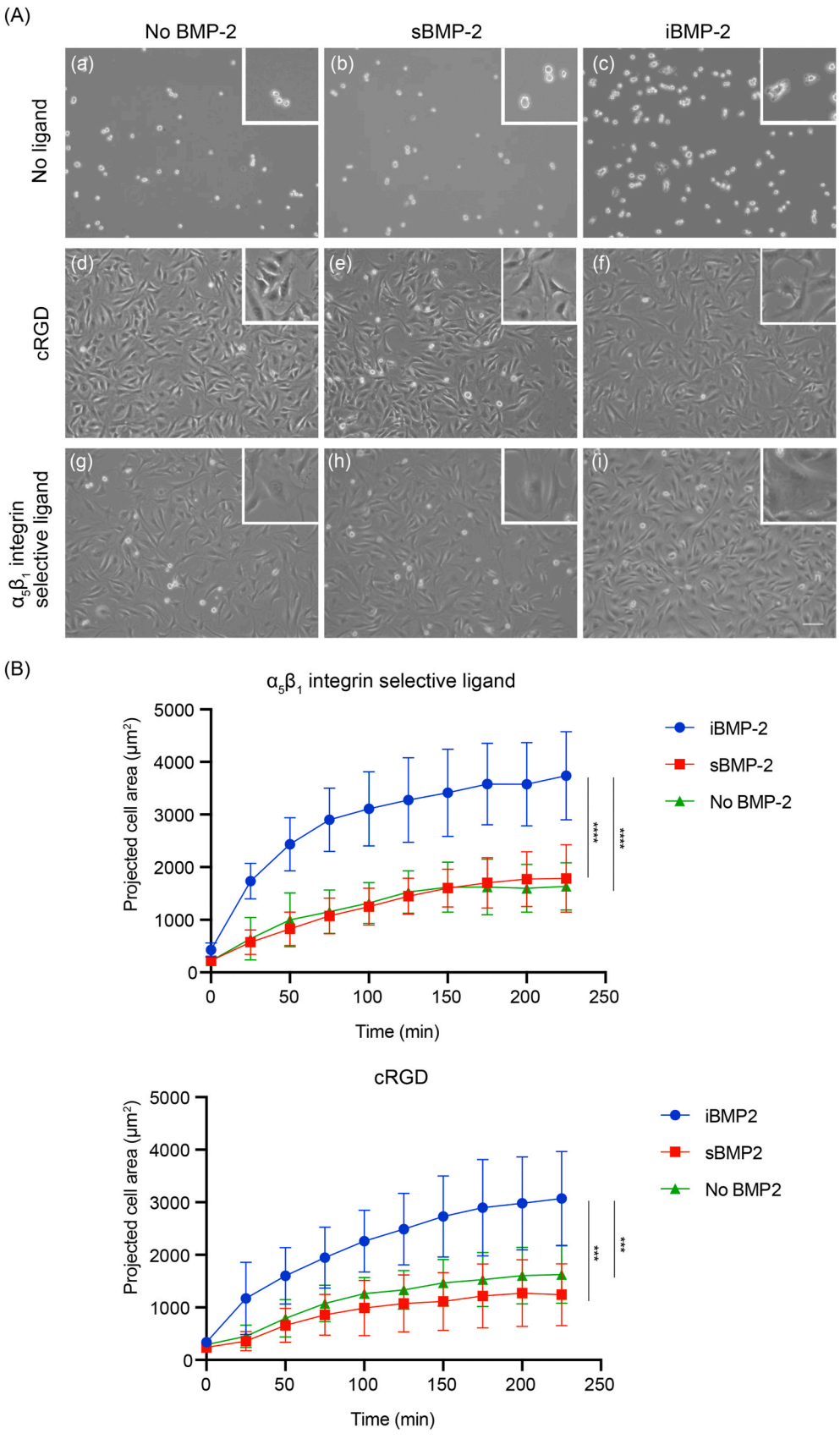

Fig. 2. Cell spreading kinetics on nanopatterned surfaces functionalized with integrin ligands and treated or not with BMP-2. (A) Representative phase contrast images of C2C12 cells 4 h after seeding on nanostructured glass surfaces used as control (a,b,c) or functionalized with cRGD adhesive ligand (d,e,f) or $\alpha_5\beta_1$ integrin selective ligand (g,h,i). C2C12 cells seeded without BMP-2 (a,d,g), with BMP-2 added to the media (b,e,h) or exposed to BMP-2 immobilized on the surfaces (c,f,i). Scale bar: 100 μm. Insets: magnification of selected areas. **(B)** Progression of projected cell area of C2C12 cells during spreading on nanopatterned surfaces functionalized with $\alpha_5\beta_1$ integrin selective ligand (upper plot) and surfaces containing cRGD adhesive ligand (lower plot) exposed to iBMP-2 (blue), sBMP-2 (red) or No BMP-2 (green). Cells seem to cover greater areas on surfaces presenting the $\alpha_5\beta_1$ integrin selective ligand; this effect of the ligand is further supported by the presence of iBMP-2 on the surfaces. For cell spreading analyses, 15 cells were analyzed per condition. Error bars indicate the standard deviation (SD) from the mean of 3 independent repeats. ***$p < 0.001$ and ****$p < 0.0001$. Data are analyzed by two-way ANOVA followed by post hoc Tukey's multiple comparisons test. . (For interpretation of the references to color in this figure legend, the reader is referred to the Web version of this article.)

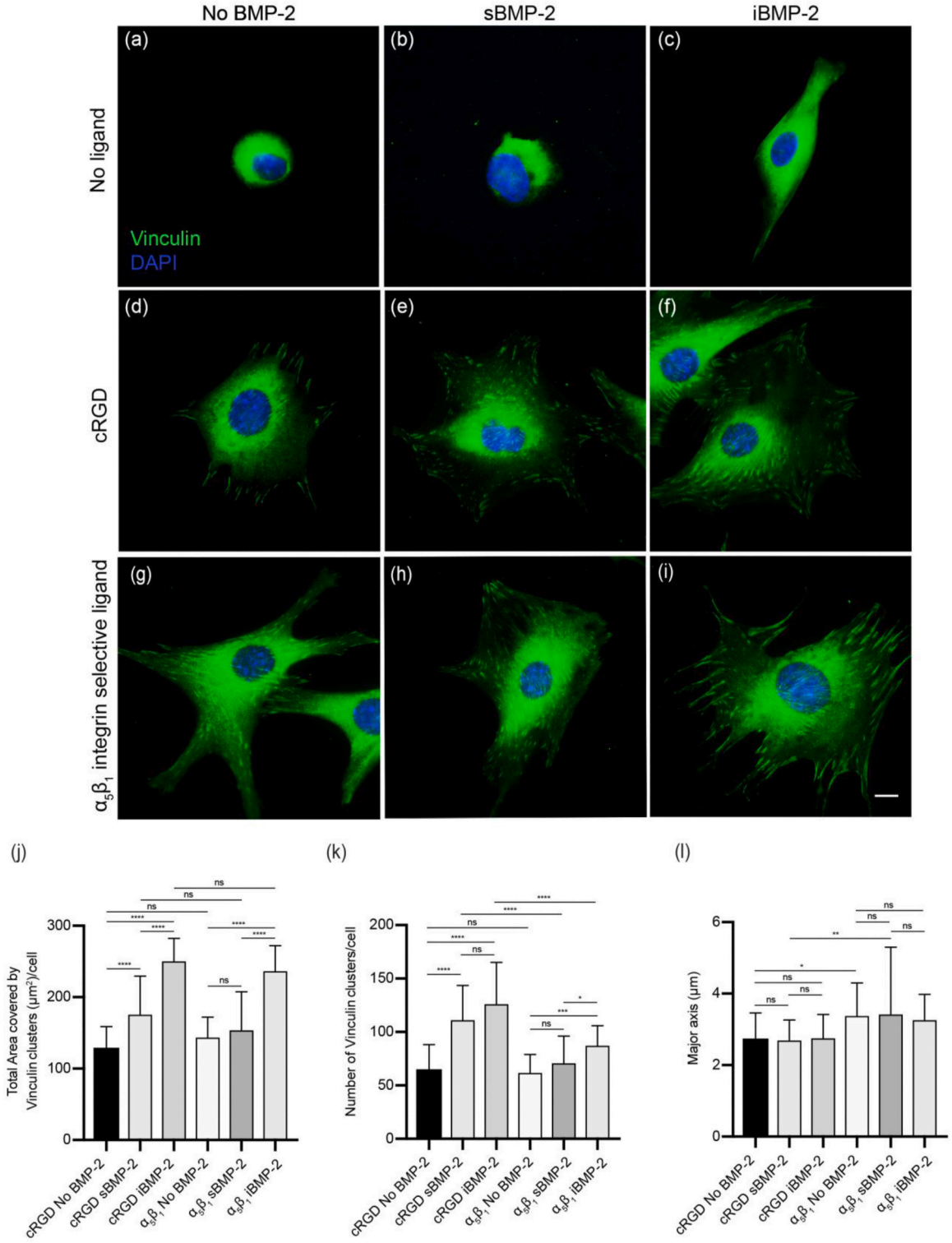

Fig. 3. FA formation in cells adhering to nanopatterned surfaces functionalized with either cRGD or $\alpha_5\beta_1$ integrin selective ligands in presence or in absence of BMP-2. Indirect immunofluorescence staining of vinculin (green) and nuclei (blue) in C2C12 cells (upper panel). Cells adhering for 4 h to nanostructured glass surfaces without the adhesive ligands are used as control (a–c); to promote cell adhesion, surfaces were functionalized with cRGD adhesive ligand (d–f) or with $\alpha_5\beta_1$ integrin selective ligand (g–i). C2C12 cells were seeded without BMP-2 (a,d,g), exposed to 5.6 ng of BMP-2 covalently immobilized on the surfaces (c,f,i), or seeded in the presence of the corresponding amount of BMP-2 in cell culture medium (b,e,h). Cells adhering to the selective $\alpha_5\beta_1$ integrin ligands with iBMP-2 (i) show evident vinculin clusters. Scale bar: 10 μm. Analysis of total area covered by FAs per cell (j), number of total FAs per cell (k) and their major axis (l). iBMP-2 enhances FA size in cells adhering to $\alpha_5\beta_1$ integrin selective ligands. Each graph represents means ± SD of 15 cells imaged for each treatment in 3 independent repeats. *$p < 0.05$, **$p < 0.01$, ***$p < 0.001$ and ****$p < 0.0001$; ns, not significant. Data are analyzed by one-way ANOVA followed by post hoc Bonferroni's multiple comparisons test. (For interpretation of the references to color in this figure legend, the reader is referred to the Web version of this article.)

surface, whereas the size is increased only for cells which bind to the surface *via* $\alpha_5\beta_1$ integrin. This might be due to the inability of β_1 integrins to translocate and form fibrillar adhesion and participate in fibronectin matrix organization. The presence of BMP-2, both when immobilized or added to the media, increases FA length and causes a decrease in the number of FAs only if copresented with $\alpha_5\beta_1$ integrin ligands.

Different integrin types and their clustering are central for driving FA formation and determining cell adhesion and spreading [47]. We next determined whether the observed effects in FA size might be due to a different recruitment of integrin subtypes and cluster organization in presence of BMP-2. The localization of β_1 and β_3 integrin subunits in cells seeded for 4 h on the different surfaces was detected by indirect immunofluorescence microscopy. For β_1 integrin localization (Fig. 4), few clusters were present mainly towards the center of cells adhering to all cRGD-functionalized samples, regardless of the presence of BMP-2 (Fig. 4, panels a–f). When adhering to $\alpha_5\beta_1$ integrin selective ligands in absence of BMP-2, cells did not assemble β_1 integrin clusters at the periphery, whereas few β_1 integrin-enriched elongated structures were present in the center (Fig. 4, panels g, j). In contrast, cells cultured on these substrates and exposed to either sBMP-2 (Fig. 4, panels h,k) or iBMP-2 (Fig. 4, panels i,l) developed at their periphery pronounced β_1 integrin clusters which were aligned with actin stress fibers. These observations were corroborated by the quantitative analysis of β_1 subunits: the total area covered by β_1 integrin clusters for each cell (Fig. 4m) and the number of clusters per cell (Fig. 4n) were both significantly higher for cells adhering to substrates presenting $\alpha_5\beta_1$ integrin selective ligand, in comparison to the samples containing cRGD. No statistical differences have been observed when comparing the effect of sBMP-2 with iBMP-2 on cells adhering to either type of integrin ligand (Fig. 4m–o). Considering the length of the major axis (Fig. 4o), although the values were comparable among the different functionalized surfaces, a statistically significant difference was observed between the samples without BMP-2 and iBMP-2. Cells adhering to $\alpha_5\beta_1$ ligand in presence of iBMP-2 formed elongated β_1 integrin-enriched clusters, which resembled fibrillar adhesions [48].

It has been recently shown [49] that upon initial engagement of $\alpha_5\beta_1$ integrins on the selective ligands, a rapid co-recruitment of $\alpha_v\beta_3$ integrins takes place to stabilize the assembly of FAs. To determine whether the presence of BMP-2, either added to the media or immobilized on the surface, might facilitate this process, we next analyzed the localization of β_3 integrin subunit in cells seeded for 4 h on the different surfaces (Fig. 5). As expected, larger peripheral β_3 integrin clusters were present in cells adhering to surfaces functionalized with cRGD (Fig. 5, panels a–f) in comparison to cells adhering to $\alpha_5\beta_1$ integrin selective ligands (Fig. 5, panels g–l). This was confirmed by the quantitative analysis of β_3 integrin clusters that showed a statistical significance between the surfaces presenting the two different adhesive ligands used (Fig. 5, panels m,n). The assembly of larger peripheral β_3 integrin clusters is in agreement with our previous findings with human osteosarcoma cells (U2OS) seeded on nanopatterned surfaces functionalized with $\alpha_5\beta_1$ and $\alpha_v\beta_3$ integrin selective ligands [34]. Moreover β_3 integrin clusters were more numerous and covered larger areas in cells treated with BMP-2 (Fig. 5, panels b–c, e-f) when compared to the control (Fig. 5, panels a,d), confirming the data shown in Fig. 3, although a statistically significant difference was observed only comparing iBMP-2 with samples without BMP-2 and sBMP-2 respectively (Fig. 5, panels m,n).

Interestingly, cells adhering to $\alpha_5\beta_1$ integrin selective ligands did not assemble any β_3 integrin clusters in absence of BMP-2 or when the growth factor was added to the culture media (Fig. 5, panels g,h,j,k). In contrast, in presence of iBMP-2, peripheral clusters could be observed (Fig. 5, panels i,l), their area (Fig. 5m) and number (Fig. 5n) were significantly higher than the ones measured for the samples in absence of BMP-2 or in presence of its soluble form, suggesting that the proximity of bound β_1 integrins and BMPRs facilitates the recruitment of non-bound β_3 integrins at FAs. It should be noted that the 4 h seeding time in 1% serum conditions, which was preceded by a 5 h starvation period, and the presence of the PEG passivating layer hinder the secretion and deposition of additional matrix proteins by cells.

Taken together these results indicate that BMP-2, either added to the culture media or immobilized on the surface, induces the assembly of peripheral β_1 integrin clusters when this integrin subunit is engaged in binding to its ligands. Moreover, for cells adhering to $\alpha_5\beta_1$ integrin ligands, the presence of iBMP-2 but not sBMP-2, induces the assembly of large β_3 integrin clusters, overcoming the selectivity imposed by $\alpha_5\beta_1$ ligand, which alone is not sufficient to induce any change in β_3 localization.

To further investigate integrin localization in presence of surface-bound BMP-2, we performed receptor blocking experiments (Fig. S2, Figs. 6 and 7). Prior to seeding, cells in suspension were incubated with the soluble form of peptidomimetic integrin ligands (Fig. S1C and D) which are able to selectively bind either to $\alpha_5\beta_1$ or $\alpha_v\beta_3$ integrins respectively [36]. The peptidomimetic $\alpha_v\beta_3$ integrin ligand has a IC_{50} ($\alpha_v\beta_3$) of 0.55 $\pm$ 0.07 nM which is much higher than the one of cRGD binding to the same integrin type (for ligand structure please see Fig. S1D) [36,39]. With the selective integrin blocking approach the ligand binding sites on integrins are occupied, although the receptors are still localized at the cell membrane and are possibly recruited at FAs in a ligand-independent way. Because of the rapid propensity of C2C12 cells to renew the integrin receptors at the cell membrane, resulting in loss of the blocking effect at 4 h (data not shown), cell adhesion and FA assembly were analyzed 2 h after seeding. Surfaces coated with fibronectin and vitronectin served as control for blocking efficiency of $\alpha_5\beta_1$ or $\alpha_v\beta_3$ integrins respectively (Fig.S2A).

The cRGD peptide has high affinity for $\alpha_v\beta_3$ integrin [50], and to a lesser extent also $\alpha_5\beta_1$ integrins can bind to it [51], but it is not a selective integrin ligand. Therefore, we could still observe adhesion after selective blocking of $\alpha_v\beta_3$ integrins (Fig.S2B upper row). Thus, in presence of the $\alpha_v\beta_3$ integrin antagonist, cells seeded on the cRGD functionalized surfaces could still engage $\alpha_5\beta_1$ integrin receptors, but a lower number of cells was able to adhere and spread. On cRGD surfaces, blocking of $\alpha_v\beta_3$ integrins affected cell adhesion and spreading for the different experimental conditions. In particular, more cells adhered after blocking of β_3 integrins only in presence of iBMP-2, supporting the findings shown in Figs. 3–5. The number of adherent cells was higher, although still not comparable to the number of cells on surfaces functionalized with $\alpha_5\beta_1$ integrin selective ligands. In contrast, following $\alpha_v\beta_3$ integrin blocking, cell spreading was not affected on surfaces presenting $\alpha_5\beta_1$ ligand, regardless of the presence of BMP-2 (Fig.S2B lower row).

To evaluate FA assembly, we performed vinculin and actin stress fiber labeling of C2C12 cells following $\alpha_v\beta_3$ integrin blocking (Fig. 6, panels a–f). On cRGD functionalized surfaces, cell spreading was reduced in comparison to cells which were not preincubated with the peptide (as shown in Fig. 3). The localization of vinculin in peripheral FAs was less pronounced in cells adhering to surfaces in absence of BMP-2 or in presence of sBMP-2 (Fig. 6, panels a and b), when compared to cells exposed to iBMP-2 (Fig. 6c). This observation was corroborated by the quantification of the total area covered by vinculin clusters (Fig. 6g) and their number (Fig. 6h), revealing a significant impact associated to the presence of iBMP-2. This feature was also evident in cells cultured on surfaces presenting the $\alpha_5\beta_1$ ligand (Fig. 6, panels d–f) and in particular when exposed to iBMP-2 (Fig. 6, panels e and f, g and h). The presence of the growth factor, presented in the immobilized form on the surfaces, favored clustering of vinculin in FAs coupled to actin stress fibers.

To determine whether $\alpha_5\beta_1$ integrin subunit was responsible for FA assembly compensating for the blocking of $\alpha_v\beta_3$ integrins, we did a co-staining for β_1 integrins (Fig. 7, panels a–f). Cells adhering to cRGD surfaces showed poor localization of β_1 integrins in FAs in all the three different conditions, regardless of the presence of BMP-2 (Fig. 7, panels a–c). Nonetheless, β_1 integrin cluster quantification showed a statistically significant increase in the total area covered by integrin clusters and in their number in the case of iBMP-2 compared to cells cultured

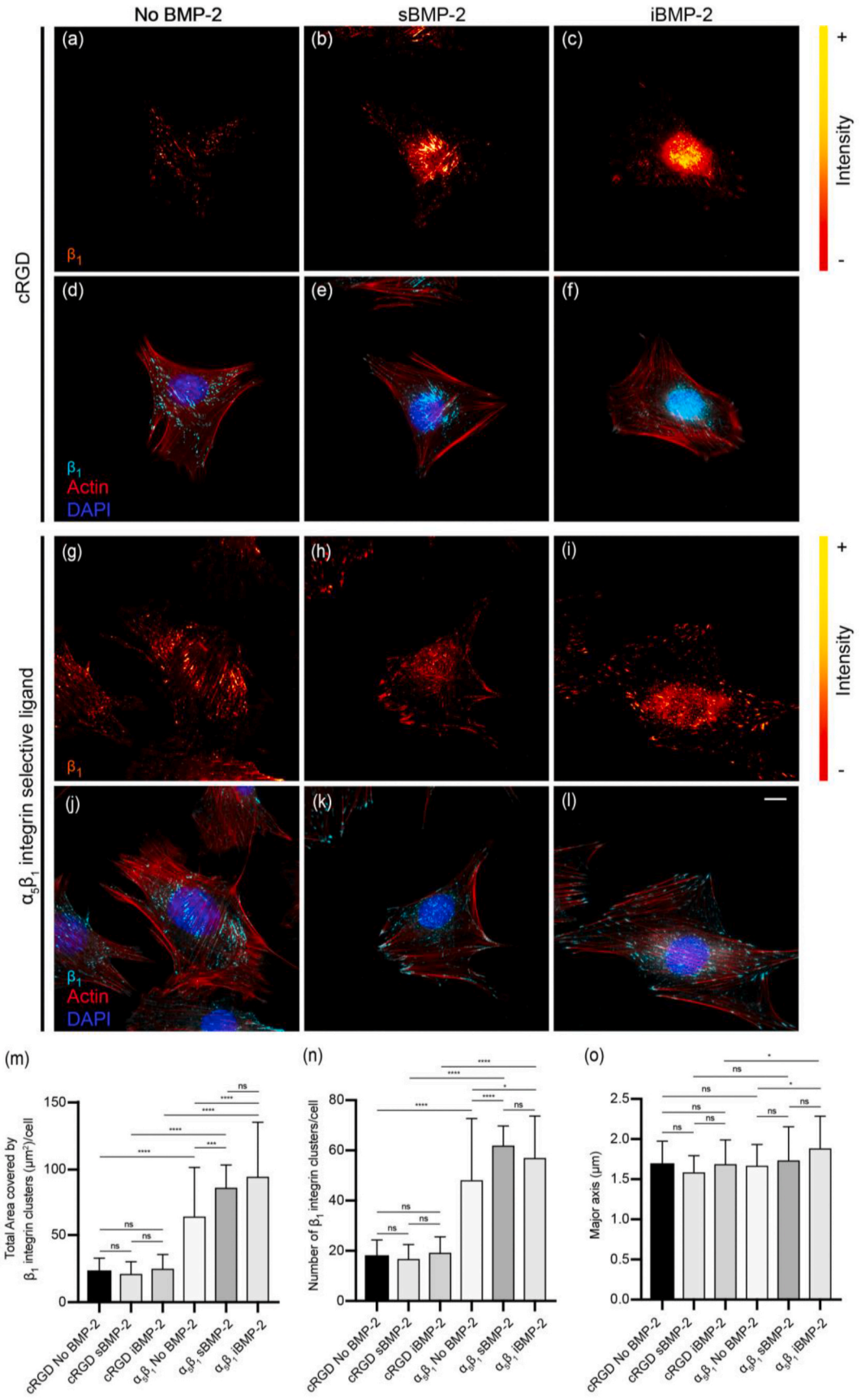

(caption on next page)

Fig. 4. BMP-2 induces clustering of β_1 integrin subunits at cell periphery when $\alpha_5\beta_1$ integrin selective ligands are present. Fluorescence microscopy images of C2C12 cells 4 h after seeding showing the localization of β_1 integrin subunits. Upper panel: cells adhering on cRGD adhesive ligands (a–f); lower panel: cells adhering on $\alpha_5\beta_1$ integrin selective ligand (g–l) immobilized on the surface by click chemistry. For each panel, upper row: lookup table displaying the localization of β_1, the color bar on the right reflects the range of pixel intensities from red (lower) to yellow (higher) (a-c,g-i); lower row: cells co-stained for β_1 integrin (cyan), actin (red) and nuclei (blue). Left: control cells without BMP-2 treatment (a,d,g,j). Middle: C2C12 cells treated with BMP-2 added to the media (b,e,h,k). Right: cells exposed to iBMP-2 (c,f,i,l). Scale bar: 10 μm. Analysis of total area covered by β_1 integrin clusters per cell (m), number of total clusters per cell (n) and their major axis (o). β_1 integrin clusters are greater and more numerous in cells adhering to $\alpha_5\beta_1$ integrin selective ligands. Each graph represents means ± SD of 15 cells imaged for each treatment in 3 independent repeats. *$p < 0.05$, **$p < 0.01$, ***$p < 0.001$ and ****$p < 0.0001$; ns, not significant. Data are analyzed by one-way ANOVA followed by post hoc Bonferroni's multiple comparisons test. (R#2, C13). (For interpretation of the references to color in this figure legend, the reader is referred to the Web version of this article.)

without the growth factor or in presence of its soluble form (Fig. 7, panels g,h). In contrast, when plated on surfaces functionalized with the $\alpha_5\beta_1$ integrin ligand, cells formed defined β_1 integrin clusters (Fig. 7, panels d–f). When iBMP-2 was present, β_1 integrin clusters covered larger areas and were more numerous in comparison to control or sBMP-2 (Fig. 7, panels f,g,h). Thus, iBMP-2, when co-presented with $\alpha_5\beta_1$ integrin selective ligands, enhances $\alpha_5\beta_1$ integrin binding and induces the formation of β_1-rich adhesions supporting cell spreading.

In summary, the selective blocking of $\alpha_v\beta_3$ integrins impairs but not prevents adhesion and spreading on cRGD and $\alpha_5\beta_1$ integrin ligands by affecting actin stress fibers formation and vinculin localization. At the same time, it has an impact on the localization and clustering of β_1 integrins, however iBMP-2 can still support and enhance FA assembly when cell adhesion is mediated only by $\alpha_5\beta_1$ integrins.

We next performed integrin blocking experiments using peptidomimetic ligands which selectively bind to $\alpha_5\beta_1$ integrins (Fig. S2C and Fig. 8). Cells seeded on surfaces functionalized with cRGD could still adhere and spread, whereas cells on surfaces presenting the $\alpha_5\beta_1$ integrin selective ligands adhered weakly 2 h after seeding, resulting in complete removal of them following gentle rinsing (Fig. S2C). Therefore it was not possible to perform indirect immunofluorescence staining of these samples. Following $\alpha_5\beta_1$ integrin blocking, cells adhering to cRGD assembled defined vinculin and β_3 integrin clusters (Fig. 8a–f). In absence of BMP-2 or when BMP-2 was added to the media (Fig. 8a,b and d,e), the clusters were localized radially and were small in size. Cells seeded on cRGD co-presented with iBMP-2 (Fig. 8c and f) were more spread and elongated vinculin clusters were present at the cell periphery, localized at the end of robust actin stress fibers. These clusters were enriched with β_3 integrins which colocalized with vinculin. The number of vinculin clusters, when iBMP-2 was present, was statistically higher if compared to both control (no BMP-2) and sBMP-2 leading to a greater area covered by FAs (Fig. 8g and h). Looking at β_3 integrin clusters quantification (Fig. 8j,k), a trend similar to the one of vinculin clusters can be observed, although a significant effect on the number of clusters was not visible, probably because it was the localization of the clusters in the cells that substantially varied. Moreover, it seems that sBMP-2 needs a functional $\alpha_5\beta_1$ to determine a higher formation of β_3 clusters, whereas iBMP-2 does not, since it was comparable to the absence of BMP-2.

3. Conclusion

In the present study we applied surface nanopatterning of GFs at a controlled surface density to determine the adhesive crosstalk between $\alpha_5\beta_1$ and $\alpha_v\beta_3$ integrins in the regulation of FA assembly. Compared to other studies, which mainly focus on BMP-mediated signaling and long term responses [52,53], with our approach based on the nanoscale spatio-chemical control of the engagement of adhesion receptors, we target BMP-mediated regulation of early cell adhesion. By using a similar immobilization strategy, applied to another GF belonging to the BMPs family, namely BMP-6, in our recent study [54] we reported how this member of the bone morphogenetic protein family enhances adhesion and signaling responses when copresented with cRGD ligands. In the present work, our approach based on the surface co-presentation of iBMP-2 and $\alpha_5\beta_1$ integrin selective ligands, allows us to unravel new functions of bone morphogenetic proteins in regulating spatial segregation of adhesion clusters and FA size mediated by specific integrin types. An intriguing aspect to be addressed in future studies is the mechanisms underlying the secondary recruitment of $\alpha_v\beta_3$ integrins in FAs induced by iBMP-2 and $\alpha_5\beta_1$ integrin selective ligands, helping in sustaining forces [55]. It shall be further considered that the assembly of β_1 integrin clusters might be favored by the combination of GF presentation and stiff environment, whereas soft matrices might enhance the physical interactions between $\alpha_v\beta_3$ integrins and BMP-2 receptors [19].

Our study provides important biological insights for a better understanding of how cell adhesion to the ECM can be locally regulated by biomimetic surfaces. This is a crucial aspect for the maintenance of cell architecture and the control of cell functions. Indeed, a key role of spatial receptor regulation is gaining more importance, for example it has been recently shown [56] that Smad activation and gene expression are facilitated and amplified when a spatial regulation of TGFβ receptors is determined by ligand-induced increased presentation at the cell surface.

The use of block copolymer micellar nanolithography to pattern growth factor and the copresentation with adhesive ligands can be further applied to perform quantitative analysis of receptor crosstalk in cells at unprecedented resolution to understand the local triggers for adhesion turnover. Furthermore, our findings may inspire the design of biomaterials to promote adhesion, based on the local and sustained presentation of GFs, while maintaining their biological activity. The deepening in the understanding of these mechanisms could support new therapeutic approaches which control the interaction of GFs with artificial materials, e.g. scaffolds and prostheses, leading to an improved tissue regeneration.

4. Experimental section

Surface nanopatterning and functionalization. Block copolymer micellar nanolithography (BCMN) was used for the preparation of surfaces, as previously reported [57,58]. Surfaces were spin-coated with a monolayer of polystyrene block-poly[2-vinylpyridine($HAuCl_4$)] diblock copolymer micelles in toluene. Based on our previous work [33], an interparticle distance of 50 nm was chosen. To prevent unspecific protein adhesion on the glass between the gold nanoparticles and to covalently bind peptides carrying an azide group, a mixture of two different types of polyethylene glycol molecules was used (PEG silane MW 2000 and Alkyne-PEG MW 3000, at a ratio of 99:1). The surfaces were then functionalized with integrin ligands, namely cRGDfK (cRGD) (Peptides International Inc, Louisville, Kentucky, USA) and $\alpha_5\beta_1$ integrin selective ligand which carry an azide function (Fig. S1) to bind to the alkyne end groups of the PEG 3000. The reaction took place during an incubation time of 2 h, in a humid chamber, at RT. Using the MU-NHS heterobifunctional linker, BMP-2 was immobilized on gold nanoparticles as previously described [32]. Carrier-free recombinant human BMP-2 expressed in *E. coli* (355 BEC/CF, R&D Systems) was used. Prior to experiments the gold nanoparticles array was characterized by scanning electron microscopy (SEM). The interparticle distance and the order parameter of the hexagonal patterns were analyzed by using a ImageJ plugin.

Cell Culture. Mouse myoblast C2C12 cells (ATCC CRL 1772) were used in this study because they do not produce endogenous BMP-2. Cells

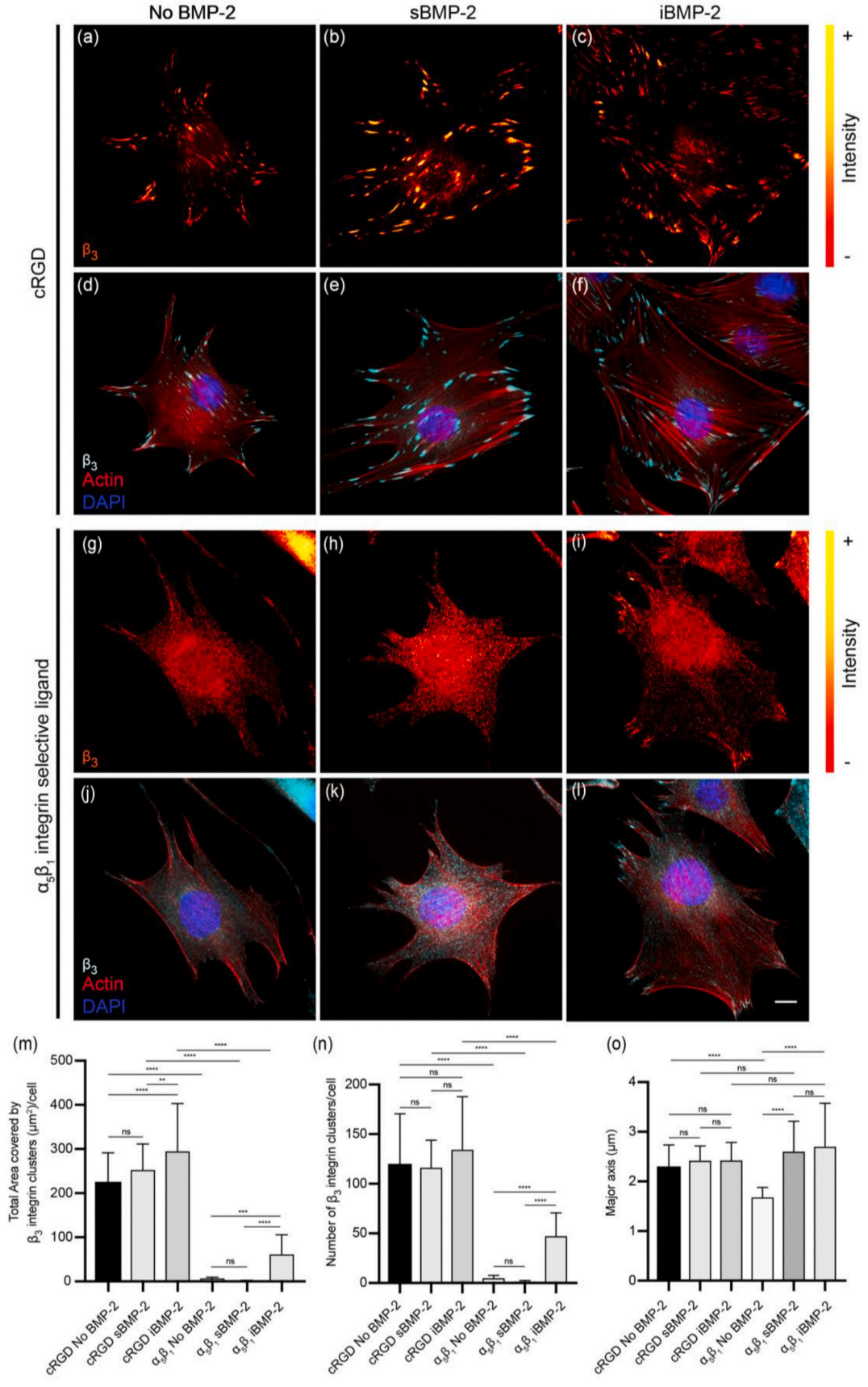

(caption on next page)

Fig. 5. The copresentation of $\alpha_5\beta_1$ integrin ligands and iBMP-2 enhances the recruitment of β_3 integrin subunits in FAs. Indirect immunofluorescence staining in C2C12 cells 4 h after seeding. Upper panel: cells adhering to cRGD adhesive ligand (a–f); lower panel: cells adhering on $\alpha_5\beta_1$ integrin selective ligand (g–l). For each panel, upper row: lookup table displaying the localization of β_3, the color bar on the right reflects the range of pixel intensities from red (lower) to yellow (higher) (a-c,g-i); lower row: immunofluorescence staining of β_3 integrin (cyan), actin (red) and nuclei (blue). Left: control cells without BMP-2 treatment (a,d,g,j). Middle: C2C12 cells treated with BMP-2 added to the media (b,e,h,k). Right: cells exposed to iBMP-2 (c,f,i,l). Scale bar: 10 μm. In the graphs, analysis of total area covered by β_3 integrin clusters per cell (m), number of total clusters per cell (n) and their major axis (o). Each graph represents means ± SD of 15 cells imaged for each treatment in 3 independent repeats. *$p < 0.05$, **$p < 0.01$, ***$p < 0.001$ and ****$p < 0.0001$; ns, not significant. Data are analyzed by one-way ANOVA followed by post hoc Bonferroni's multiple comparisons test. (For interpretation of the references to color in this figure legend, the reader is referred to the Web version of this article.)

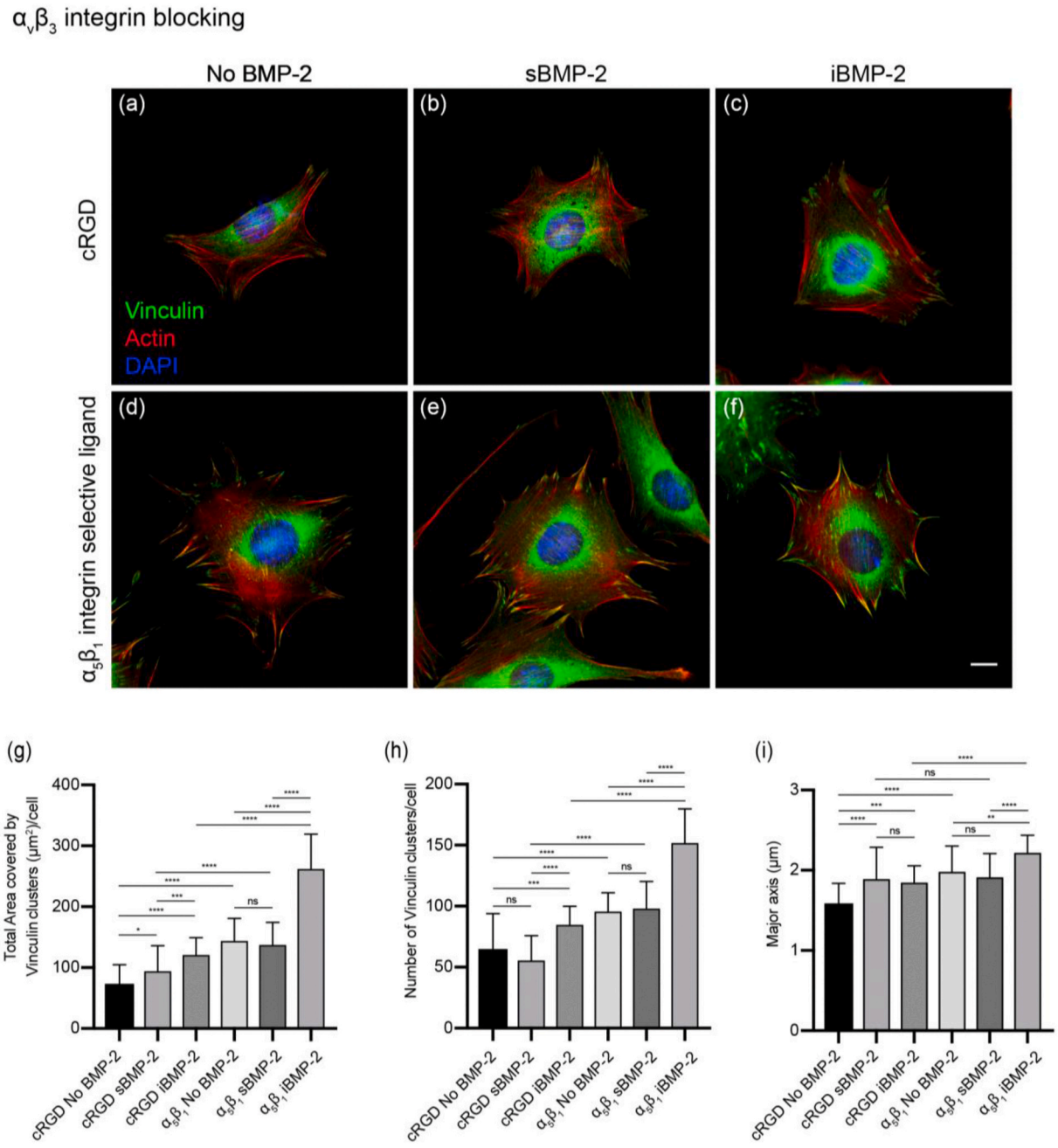

Fig. 6. $\alpha_v\beta_3$ integrin is dispensable for iBMP-2-mediated effects on FA assembly. Fluorescent micrographs of representative C2C12 cells 2 h after seeding in $\alpha_v\beta_3$ integrin blocking experiments and their quantification. Immunofluorescence staining of vinculin (green), actin (red) and nuclei (blue). Upper row: cells adhering on cRGD adhesive ligand (a–c); lower row: cells adhering on $\alpha_5\beta_1$ integrin selective ligand (d–f). Left: control cells without BMP-2 treatment (a,d). Middle: C2C12 cells treated with BMP-2 added to the media (b,e). Right: cells exposed to iBMP-2 (c,f). Scale bar: 10 μm. In the graphs, analysis of total area covered by vinculin clusters per cell (g), number of total clusters per cell (h) and their major axis (i). iBMP-2 enhances FA size and number in cells adhering to $\alpha_5\beta_1$ integrin selective ligands. Each graph represents means ± SD of 15 cells imaged for each treatment in 3 independent repeats. *$p < 0.05$, **$p < 0.01$, ***$p < 0.001$ and ****$p < 0.0001$; ns, not significant. Data are analyzed by one-way ANOVA followed by post hoc Bonferroni's multiple comparisons test. (For interpretation of the references to color in this figure legend, the reader is referred to the Web version of this article.)

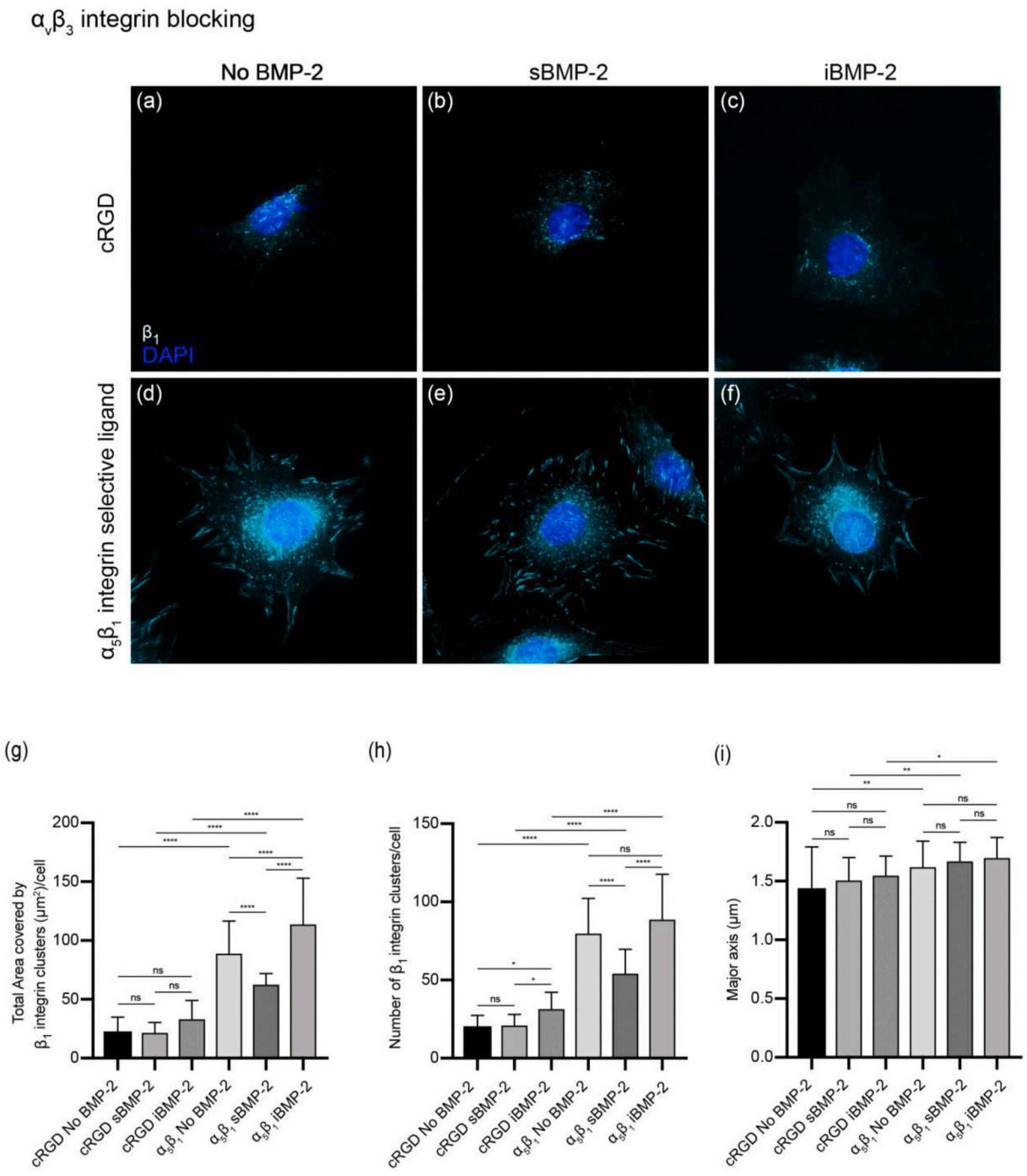

Fig. 7. Fluorescent micrographs of representative C2C12 cells after $\alpha_v\beta_3$ integrin blocking and their quantification. Indirect immunofluorescence staining in C2C12 cells 2 h after seeding on nanopatterned surfaces functionalized with cRGD adhesive ligand (a–c) or $\alpha_5\beta_1$ integrin selective ligand (d–f). Cells co-stained for β_3 integrin (cyan) and nuclei (blue). Left: control cells without BMP-2 treatment (a and d). Middle: C2C12 cells treated with BMP-2 added to the media (b and e). Right: cells exposed to iBMP-2 (c and f). Scale bar: 10 μm. In the graphs, analysis of total area covered by β_1 integrin clusters per cell (g), number of total clusters per cell (h) and their major axis (i). iBMP-2, coupled with $\alpha_5\beta_1$ integrin selective ligands, induces β_1 clustering. Each graph represents means ± SD of 15 cells imaged for each treatment in 3 independent repeats. *$p < 0.05$, **$p < 0.01$, ***$p < 0.001$ and ****$p < 0.0001$; ns, not significant. Data are analyzed by one-way ANOVA followed by post hoc Bonferroni's multiple comparisons test). (For interpretation of the references to color in this figure legend, the reader is referred to the Web version of this article.)

were cultured in D-MEM (Thermo Fisher Scientific) supplemented with 10% fetal bovine serum (FBS), 100 U/ml penicillin-G and 100 μg/ml streptomycin (Thermo Fisher Scientific) as sub-confluent monolayer, at 37 °C and 5% CO_2. The medium was renewed every 3 days. Upon reaching 70–80% confluence, cells were serum starved for 5 h, and then detached with 0.05% Trypsin/EDTA (Thermo Fisher Scientific). C2C12 cells, with a number of passages lower than nine, were seeded on the nanopatterned surfaces at density of 20×10^3 cells/cm^2 in D-MEM supplemented with 1% FBS. For time lapse phase contrast microscopy, cells were maintained in a temperature controlled chamber with 5% of CO_2; one image was acquired every 5 min with a 20x objective for a period of 4 h.

Integrin blocking experiments. C2C12 cells were resuspended in D-MEM supplemented with 1% FBS and 1% BSA at cell density of 1×10^6

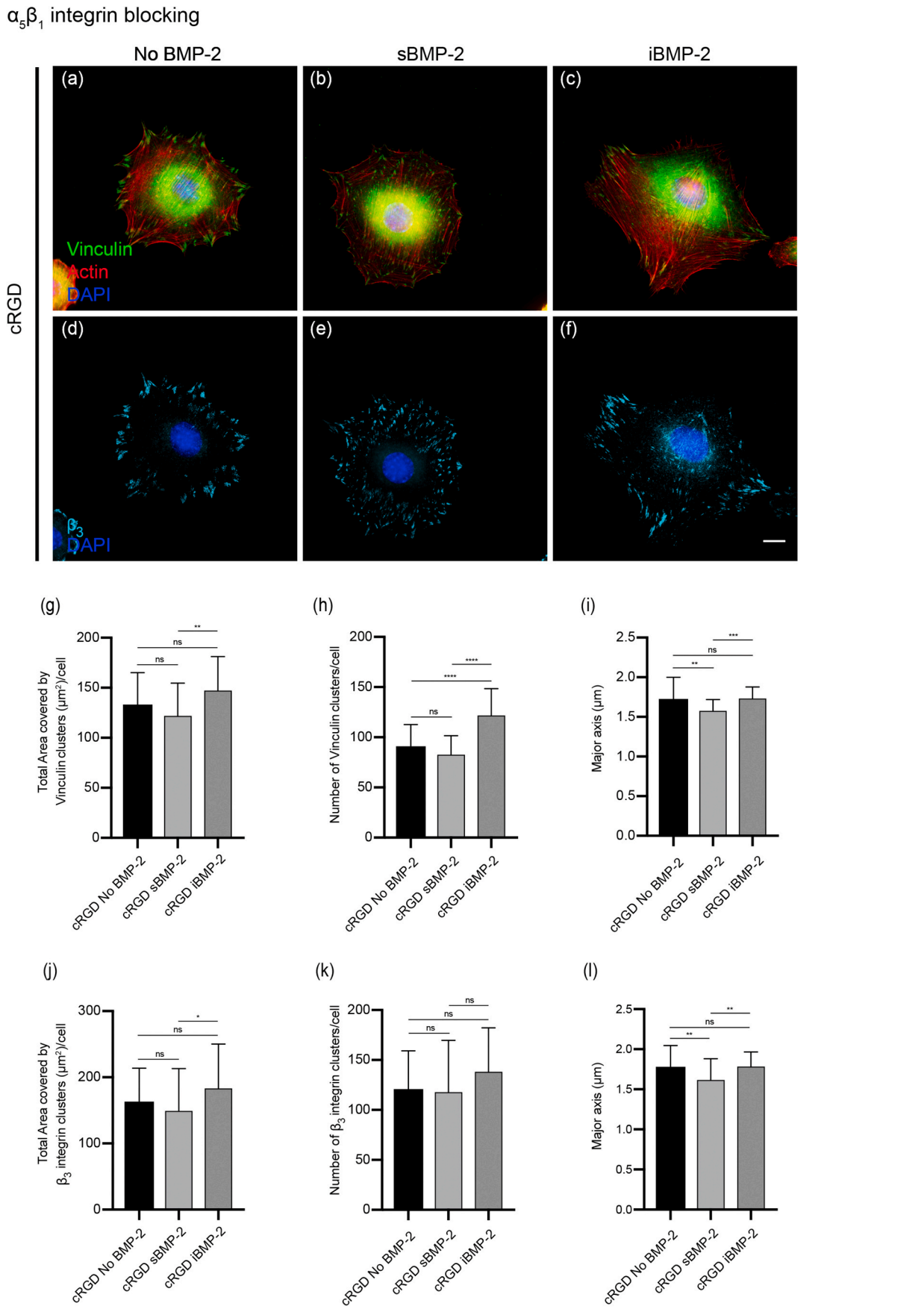

(caption on next page)

Fig. 8. Fluorescent micrographs of representative C2C12 cells after $\alpha_5\beta_1$ integrin blocking and their quantification. Indirect immunofluorescence staining in C2C12 cells 2 h after seeding on nanopatterned surfaces functionalized with cRGD adhesive ligand (a–f). Upper row: immunofluorescence staining of vinculin (green), actin (red) and nuclei (blue) (a–c). Lower row: β_3 integrin (cyan) and nuclei (blue) (d–f). Left: control cells without BMP-2 treatment (a and d). Middle: C2C12 cells treated with BMP-2 added to the media (b and e). Right: cells exposed to iBMP-2 (c and f). Scale bar: 10 μm. In the graphs, analysis of total area covered by vinculin or β_3 integrin clusters per cell (g and j), number of total clusters per cell (h and k) and their major axis (i and l). iBMP-2 favors the spatial segregation of β_3 integrin clusters (f). Each graph represents means ± SD of 15 cells imaged for each treatment in 3 independent repeats. *$p < 0.05$, **$p < 0.01$, ***$p < 0.001$ and ****$p < 0.0001$; ns, not significant. Data are analyzed by one-way ANOVA followed by post hoc Bonferroni's multiple comparisons test. (For interpretation of the references to color in this figure legend, the reader is referred to the Web version of this article.)

cells/ml. Then cells were incubated on ice for 1 h in presence of azide-free ligands [36] (10 μM) added to the medium, using 75 μl of the azide-free ligand for each 100 μl of cell suspension. Cells were then seeded on the surfaces functionalized or not with cRGD or $\alpha_5\beta_1$ integrin selective ligand. Fibronectin and vitronectin served as control; these ECM proteins were from Sigma Aldrich, St. Louis, MO, USA (F1141 and V8379). After 2 h the samples were gently rinsed with PBS for removing non-adherent cells and then fixed and stained for microscopy analysis.

Indirect Immunofluorescence, microscopy image acquisition and analysis. C2C12 cells were starved for 5 h, then seeded at a density of 20×10^3 cells/cm^2 on surfaces prepared as previously described and cultured in 1% FBS D-MEM. At the indicated time points, cells were fixed with 4% (PFA)/PBS for 15 min. After washing twice with PBS, cell permeabilization was performed in 0.1% TRITON-X 100 in PBS, then blocking was achieved by incubating the samples in 1% BSA in PBS for 1 h. The samples were incubated with the following antibodies: Vinculin, β_3, β_1. Anti-vinculin antibody was from Sigma Aldrich (V9131), anti-integrin β_1 was from BD Biosciences (550531), anti-integrin β_3 was from Emfret Analytics (M03-0 Clone LucA5). After washing, the bound antibody was detected using fluorescently labeled anti-mouse Alexa fluor 488 or anti-rat Alexa fluor 647 secondary antibodies from Thermo Fisher Scientific (A-11001 and A-21247); cytoskeleton was counter-stained with phalloidin-TRITC (P1951, Sigma Aldrich). A DeltaVision (DV) microscope (Applied Precision Inc., Canada; data processing controlled by Resolve 3D (Applied Precision Inc., USA)) was used to image cells. The images were adjusted in brightness and color with ImageJ software (Research Services Branch, Image Analysis Software Version 1.53a, NIH, Bethesda, MD, USA). The FA quantitative analysis was performed by using a protocol described in U. Horzum U et al. [46].

Statistical analysis. Statistical analysis was carried out for 45 cells per condition (for each condition, 15 cells were analyzed and each experiment was repeated three times). All plotted data show mean values with standard deviations calculated from three independent experiments. Statistical calculations were performed using GraphPad Prism version 7.0d for Mac OS X (GraphPad Software, La Jolla California USA, www.graphpad.com). The results were considered statistically significant for $p < 0.05$.

Funding

This research was funded by grants from the German Science Foundation—project number 107540325—SFB TRR 79 project B05 to E.A.C.-A.; by the European Union Horizon 2020 research and innovation programme (Marie Skłodowska-Curie grant No 872869) to E.A.C.-A.; by ANR grant (ANR-17-CE13-022) and FRM grant (DEQ20170336702) to C.AR.

Data availability statement

The raw/processed data required to reproduce these findings cannot be shared at this time due to technical limitations. However data can be shared upon direct request to the authors.

CRediT authorship contribution statement

Francesca Posa: Conceptualization, Formal analysis, Investigation, Methodology, Visualization, Writing - original draft, Writing - review & editing. **Elisabeth H. Baha-Schwab:** Investigation, Visualization, Writing - review & editing. **Qiang Wei:** Methodology, Writing - review & editing. **Adriana Di Benedetto:** Methodology, Writing - review & editing. **Stefanie Neubauer:** Methodology, Writing - review & editing. **Florian Reichart:** Methodology, Writing - review & editing. **Horst Kessler:** Methodology, Resources, Writing - review & editing. **Joachim P. Spatz:** Resources, Writing - review & editing. **Corinne Albiges-Rizo:** Conceptualization, Writing - review & editing. **Giorgio Mori:** Methodology, Supervision, Writing - original draft, Writing - review & editing. **Elisabetta Ada Cavalcanti-Adam:** Conceptualization, Formal analysis, Funding acquisition, Project administration, Resources, Supervision, Writing - original draft, Writing - review & editing.

Declaration of competing interest

The authors declare that they have no known competing financial interests or personal relationships that could have appeared to influence the work reported in this paper.

Acknowledgements

FP, QW, JPS and EAC-A acknowledge the support from the Max Planck Society. The authors thank Dr. Anna Luise Grab, Dr. Jie Li, Dr. Tobias Kapp, Mrs. Sabine Grünewald, Mr. Ioanis Grigoridis and Mrs. Maria Sycha for support and discussions. We also thank Dr. Philipp Girard (Institut Jacques Monod Paris, France) for developing the ImageJ plugin to measure the order parameter and the interparticle distance of the nanopatterned substrates.

Appendix A. Supplementary data

Supplementary data to this article can be found online at https://doi.org/10.1016/j.biomaterials.2020.120484.

Abbreviations

ECM	extracellular matrix
GFs	growth factors
FAs	focal adhesions
BMPR	bone morphogenetic protein receptor
BCMN	block-copolymer micellar nanolithography
rhBMP-2	recombinant human bone morphogenetic protein-2
BSA	bovine serum albumin
iBMP-2	immobilized bone morphogenetic protein-2
PEG	polyethylene glycol
MU-NHS	11-mercaptoundecanoyl-*N*-hydroxysuccinimide ester
sBMP-2	soluble bone morphogenetic protein-2
SEM	scanning electron microscopy
TGF-β	transforming growth factor-β

References

[1] C. Frantz, K.M. Stewart, V.M. Weaver, The extracellular matrix at a glance, J. Cell Sci. 123 (Pt 24) (2010) 4195–4200, https://doi.org/10.1242/jcs.023820.
[2] K.C. Clause, T.H. Barker, Extracellular matrix signaling in morphogenesis and repair, Curr. Opin. Biotechnol. 24 (5) (2013) 830–833, https://doi.org/10.1016/j.copbio.2013.04.011.

[3] A.D. Theocharis, S.S. Skandalis, C. Gialeli, N.K. Karamanos, Extracellular matrix structure, Adv. Drug Deliv. Rev. 97 (2016) 4–27, https://doi.org/10.1016/j.addr.2015.11.001.

[4] R.O. Hynes, The extracellular matrix: not just pretty fibrils, Science 326 (5957) (2009) 1216–1219, https://doi.org/10.1126/science.1176009.

[5] M.M. Martino, J.A. Hubbell, The 12th–14th type III repeats of fibronectin function as a highly promiscuous growth factor-binding domain, Faseb. J. 24 (12) (2010) 4711–4721.

[6] S.M. Schoenwaelder, K. Burridge, Bidirectional signaling between the cytoskeleton and integrins, Curr. Opin. Cell Biol. 11 (2) (1999) 274–286.

[7] K.M. Yamada, B. Geiger, Molecular interactions in cell adhesion complexes, Curr. Opin. Cell Biol. 9 (1) (1997) 76–85.

[8] C. Albiges-Rizo, O. Destaing, B. Fourcade, E. Planus, M.R. Block, Actin machinery and mechanosensitivity in invadopodia, podosomes and focal adhesions, J. Cell Sci. 122 (17) (2009) 3037–3049, https://doi.org/10.1242/jcs.052704.

[9] F. Karimi, A.J. O'Connor, G.G. Qiao, D.E. Heath, Integrin clustering matters: a review of biomaterials functionalized with multivalent integrin-binding ligands to improve cell adhesion, migration, differentiation, angiogenesis, and biomedical device integration, Advanced healthcare materials 7 (12) (2018), e1701324, https://doi.org/10.1002/adhm.201701324.

[10] S. Tadokoro, S.J. Shattil, K. Eto, V. Tai, R.C. Liddington, J.M. de Pereda, M. H. Ginsberg, D.A. Calderwood, Talin binding to integrin ß tails: a final common step in integrin activation, Science 302 (5642) (2003) 103–106.

[11] M.A. Schwartz, Integrins and extracellular matrix in mechanotransduction, Cold Spring Harbor perspectives in biology (2010) a005066, https://doi.org/10.1101/cshperspect.a005066.

[12] A. Di Benedetto, G. Brunetti, F. Posa, A. Ballini, F.R. Grassi, G. Colaianni, S. Colucci, E. Rossi, E.A. Cavalcanti-Adam, L. Lo Muzio, M. Grano, G. Mori, Osteogenic differentiation of mesenchymal stem cells from dental bud: role of integrins and cadherins, Stem Cell Res. 15 (3) (2015) 618–628, https://doi.org/10.1016/j.scr.2015.09.011.

[13] F. Posa, A. Di Benedetto, G. Colaianni, E.A. Cavalcanti-Adam, G. Brunetti, C. Porro, T. Trotta, M. Grano, G. Mori, Vitamin D effects on osteoblastic differentiation of mesenchymal stem cells from dental tissues, Stem Cell. Int. 2016 (2016) 9150819, https://doi.org/10.1155/2016/9150819.

[14] F. Posa, A. Di Benedetto, E.A. Cavalcanti-Adam, G. Colaianni, C. Porro, T. Trotta, G. Brunetti, L. Lo Muzio, M. Grano, G. Mori, Vitamin D promotes MSC osteogenic differentiation stimulating cell adhesion and alphaVbeta3 expression, Stem Cell. Int. 2018 (2018) 6958713, https://doi.org/10.1155/2018/6958713.

[15] A. Di Benedetto, F. Posa, S. De Maria, G. Ravagnan, A. Ballini, C. Porro, T. Trotta, M. Grano, L.L. Muzio, G. Mori, Polydatin, natural precursor of resveratrol, promotes osteogenic differentiation of mesenchymal stem cells, Int. J. Med. Sci. 15 (9) (2018) 944–952, https://doi.org/10.7150/ijms.24111.

[16] Q. Wei, T.L. Pohl, A. Seckinger, J.P. Spatz, E.A. Cavalcanti-Adam, Regulation of integrin and growth factor signaling in biomaterials for osteodifferentiation, Beilstein J. Org. Chem. 11 (1) (2015) 773–783, https://doi.org/10.3762/bjoc.11.87.

[17] T.C. Nichols, T.d. Laney, B. Zheng, D.A. Bellinger, G.A. Nickols, W. Engleman, D. R. Clemmons, Reduction in atherosclerotic lesion size in pigs by αvβ3 inhibitors is associated with inhibition of insulin-like growth factor-I–mediated signaling, Circ. Res. 85 (11) (1999) 1040–1045.

[18] A. Mariotti, P.A. Kedeshian, M. Dans, A.M. Curatola, L. Gagnoux-Palacios, F. G. Giancotti, EGF-R signaling through Fyn kinase disrupts the function of integrin α6β4 at hemidesmosomes: role in epithelial cell migration and carcinoma invasion, J. Cell Biol. 155 (3) (2001) 447–458, https://doi.org/10.1083/jcb.200105017.

[19] L. Fourel, A. Valat, E. Faurobert, R. Guillot, I. Bourrin-Reynard, K. Ren, L. Lafanechère, E. Planus, C. Picart, C. Albiges-Rizo, β3 integrin–mediated spreading induced by matrix-bound BMP-2 controls Smad signaling in a stiffness-independent manner, J. Cell Biol. 212 (6) (2016) 693–706, https://doi.org/10.1083/jcb.201508018.

[20] T. Crouzier, L. Fourel, T. Boudou, C. Albigès-Rizo, C. Picart, Presentation of BMP-2 from a soft biopolymeric film unveils its activity on cell adhesion and migration, Adv. Mater. 23 (12) (2011) H111–H118, https://doi.org/10.1002/adma.201004637.

[21] R. Agarwal, A.J. García, Biomaterial strategies for engineering implants for enhanced osseointegration and bone repair, Adv. Drug Deliv. Rev. 94 (2015) 53–62, https://doi.org/10.1016/j.addr.2015.03.013.

[22] K. Kashiwagi, T. Tsuji, K. Shiba, Directional BMP-2 for functionalization of titanium surfaces, Biomaterials 30 (6) (2009) 1166–1175, https://doi.org/10.1016/j.biomaterials.2008.10.040.

[23] A. Hayrapetyan, J.A. Jansen, J.J. van den Beucken, Signaling pathways involved in osteogenesis and their application for bone regenerative medicine, Tissue Eng. B Rev. 21 (1) (2014) 75–87, https://doi.org/10.1089/ten.TEB.2014.0119.

[24] C. Sieber, J. Kopf, C. Hiepen, P. Knaus, Recent advances in BMP receptor signaling, Cytokine Growth Factor Rev. 20 (5–6) (2009) 343–355, https://doi.org/10.1016/j.cytogfr.2009.10.007.

[25] B.B. Koenig, J.S. Cook, D.H. Wolsing, J. Ting, J.P. Tiesman, P.E. Correa, C.A. Olson, A.L. Pecquet, F. Ventura, R.A. Grant, Characterization and cloning of a receptor for BMP-2 and BMP-4 from NIH 3T3 cells, Mol. Cell Biol. 14 (9) (1994) 5961–5974.

[26] A.K. Shah, J. Lazatin, R.K. Sinha, T. Lennox, N.J. Hickok, R.S. Tuan, Mechanism of BMP-2 stimulated adhesion of osteoblastic cells to titanium alloy, Biol. Cell. 91 (2) (1999) 131–142.

[27] L. Nissinen, L. Pirila, J. Heino, Bone morphogenetic protein-2 is a regulator of cell adhesion, Exp. Cell Res. 230 (2) (1997) 377–385, https://doi.org/10.1006/excr.1996.3438.

[28] C. Gamell, N. Osses, R. Bartrons, T. Rückle, M. Camps, J.L. Rosa, F. Ventura, BMP2 induction of actin cytoskeleton reorganization and cell migration requires PI3-kinase and Cdc42 activity, J. Cell Sci. 121 (23) (2008) 3960–3970, https://doi.org/10.1242/jcs.031286.

[29] E. Migliorini, A. Valat, C. Picart, E.A. Cavalcanti-Adam, Tuning cellular responses to BMP-2 with material surfaces, Cytokine Growth Factor Rev. 27 (2016) 43–54, https://doi.org/10.1016/j.cytogfr.2015.11.008.

[30] M.M. Martino, F. Tortelli, M. Mochizuki, S. Traub, D. Ben-David, G.A. Kuhn, R. Müller, E. Livne, S.A. Eming, J.A. Hubbell, Engineering the growth factor microenvironment with fibronectin domains to promote wound and bone tissue healing, Sci. Transl. Med. 3 (100) (2011) 100ra89, https://doi.org/10.1126/scitranslmed.3002614.

[31] I. Bilem, L. Plawinski, P. Chevallier, C. Ayela, E.D. Sone, G. Laroche, M.C. Durrieu, The spatial patterning of RGD and BMP-2 mimetic peptides at the subcellular scale modulates human mesenchymal stem cells osteogenesis, J. Biomed. Mater. Res. 106 (4) (2018) 959–970, https://doi.org/10.1002/jbm.a.36296.

[32] T.L. Pohl, J.H. Boergermann, G.K. Schwaerzer, P. Knaus, E.A. Cavalcanti-Adam, Surface immobilization of bone morphogenetic protein 2 via a self-assembled monolayer formation induces cell differentiation, Acta Biomater. 8 (2) (2012) 772–780, https://doi.org/10.1016/j.actbio.2011.10.019.

[33] E.H. Schwab, T.L. Pohl, T.s. Haraszti, G.K. Schwaerzer, C. Hiepen, J.P. Spatz, P. Knaus, E.A. Cavalcanti-Adam, Nanoscale control of surface immobilized BMP-2: toward a quantitative assessment of BMP-mediated signaling events, Nano Lett. 15 (3) (2015) 1526–1534, https://doi.org/10.1021/acs.nanolett.5b00315.

[34] V. Schaufler, H. Czichos-Medda, V. Hirschfeld-Warnecken, S. Neubauer, F. Rechenmacher, R. Medda, H. Kessler, B. Geiger, J.P. Spatz, E.A. Cavalcanti-Adam, Selective binding and lateral clustering of α5β1 and αvβ3 integrins: unraveling the spatial requirements for cell spreading and focal adhesion assembly, Cell Adhes. Migrat. 10 (5) (2016) 505–515, https://doi.org/10.1080/19336918.2016.1163453.

[35] C. Mas-Moruno, R. Fraioli, F. Rechenmacher, S. Neubauer, T.G. Kapp, H. Kessler, alphavbeta3- or alpha5beta1-integrin-selective peptidomimetics for surface coating, Angew. Chem. 55 (25) (2016) 7048–7067, https://doi.org/10.1002/anie.201509782.

[36] F. Rechenmacher, S. Neubauer, J. Polleux, C. Mas-Moruno, M. De Simone, E. A. Cavalcanti-Adam, J.P. Spatz, R. Fässler, H. Kessler, Functionalizing αvβ3-or α5β1-selective integrin antagonists for surface coating: a method to discriminate integrin subtypes in vitro, Angew. Chem. Int. Ed. 52 (5) (2013) 1572–1575, https://doi.org/10.1002/anie.201206370.

[37] E.A. Cavalcanti-Adam, T. Volberg, A. Micoulet, H. Kessler, B. Geiger, J.P. Spatz, Cell spreading and focal adhesion dynamics are regulated by spacing of integrin ligands, Biophys. J. 92 (8) (2007) 2964–2974, https://doi.org/10.1529/biophysj.106.089730.

[38] F.C. Schenk, H. Boehm, J.P. Spatz, S.V. Wegner, Dual-functionalized nanostructured biointerfaces by click chemistry, Langmuir 30 (23) (2014) 6897–6905, https://doi.org/10.1021/la500766t.

[39] T.G. Kapp, F. Rechenmacher, S. Neubauer, O.V. Maltsev, E.A. Cavalcanti-Adam, R. Zarka, U. Reuning, J. Notni, H.J. Wester, C. Mas-Moruno, J. Spatz, B. Geiger, H. Kessler, A comprehensive evaluation of the activity and selectivity profile of ligands for RGD-binding integrins, Sci. Rep. 7 (2017) 39805, https://doi.org/10.1038/srep39805.

[40] V. Karageorgiou, L. Meinel, S. Hofmann, A. Malhotra, V. Volloch, D. Kaplan, Bone morphogenetic protein-2 decorated silk fibroin films induce osteogenic differentiation of human bone marrow stromal cells, J. Biomed. Mater. Res. Part A: An Official Journal of The Society for Biomaterials, The Japanese Society for Biomaterials, and The Australian Society for Biomaterials and the Korean Society for Biomaterials 71 (3) (2004) 528–537, https://doi.org/10.1002/jbm.a.30186.

[41] V. Luginbuehl, L. Meinel, H.P. Merkle, B. Gander, Localized delivery of growth factors for bone repair, Eur. J. Pharm. Biopharm. : official journal of Arbeitsgemeinschaft fur Pharmazeutische Verfahrenstechnik e.V 58 (2) (2004) 197–208, https://doi.org/10.1016/j.ejpb.2004.03.004.

[42] K.S. Masters, Covalent growth factor immobilization strategies for tissue repair and regeneration, Macromol. Biosci. 11 (9) (2011) 1149–1163, https://doi.org/10.1002/mabi.201000505.

[43] R. Goncalves, M.C. Martins, M.J. Oliveira, G. Almeida-Porada, M.A. Barbosa, Bioactivity of immobilized EGF on self-assembled monolayers: optimization of the immobilization process, J. Biomed. Mater. Res. 94 (2) (2010) 576–585, https://doi.org/10.1002/jbm.a.32723.

[44] K. Hauff, C. Zambarda, M. Dietrich, M. Halbig, A.L. Grab, R. Medda, E. A. Cavalcanti-Adam, Matrix-immobilized BMP-2 on microcontact printed fibronectin as an in vitro tool to study BMP-mediated signaling and cell migration, Frontiers in bioengineering and biotechnology 3 (2015) 62, https://doi.org/10.3389/fbioe.2015.00062.

[45] B. Geiger, K. Tokuyasu, A.H. Dutton, S. Singer, Vinculin, an intracellular protein localized at specialized sites where microfilament bundles terminate at cell membranes, Proc. Natl. Acad. Sci. Unit. States Am. 77 (7) (1980) 4127–4131.

[46] U. Horzum, B. Ozdil, D. Pesen-Okvur, Step-by-step quantitative analysis of focal adhesions, MethodsX 1 (2014) 56–59, https://doi.org/10.1016/j.mex.2014.06.004.

[47] M.A. Wozniak, K. Modzelewska, L. Kwong, P.J. Keely, Focal adhesion regulation of cell behavior, Biochim. Biophys. Acta 1692 (2–3) (2004) 103–119, https://doi.org/10.1016/j.bbamcr.2004.04.007.

[48] E. Zamir, M. Katz, Y. Posen, N. Erez, K.M. Yamada, B.Z. Katz, S. Lin, D.C. Lin, A. Bershadsky, Z. Kam, B. Geiger, Dynamics and segregation of cell-matrix adhesions in cultured fibroblasts, Nat. Cell Biol. 2 (4) (2000) 191–196, https://doi.org/10.1038/35008607.

[49] C. Diaz, S. Neubauer, F. Rechenmacher, H. Kessler, D. Missirlis, Recruitment of α(ν)β(3) integrin to α(5)β(1) integrin-induced clusters enables focal adhesion maturation and cell spreading, J. Cell Sci. 133 (1) (2020), https://doi.org/10.1242/jcs.232702.
[50] J.D. Humphries, A. Byron, M.J. Humphries, Integrin ligands at a glance, J. Cell Sci. 119 (19) (2006) 3901–3903, https://doi.org/10.1242/jcs.03098.
[51] E. Zamir, B. Geiger, Components of cell-matrix adhesions, J. Cell Sci. 114 (20) (2001) 3577–3579.
[52] M.-J. Kim, B. Lee, K. Yang, J. Park, S. Jeon, S.H. Um, D.-I. Kim, S.G. Im, S.-W. Cho, BMP-2 peptide-functionalized nanopatterned substrates for enhanced osteogenic differentiation of human mesenchymal stem cells, Biomaterials 34 (30) (2013) 7236–7246, https://doi.org/10.1016/j.biomaterials.2013.06.019.
[53] I. Bilem, P. Chevallier, L. Plawinski, E.D. Sone, M.C. Durrieu, G. Laroche, RGD and BMP-2 mimetic peptide crosstalk enhances osteogenic commitment of human bone marrow stem cells, Acta Biomater. 36 (2016) 132–142, https://doi.org/10.1016/j.actbio.2016.03.032.
[54] F. Posa, A.L. Grab, V. Martin, D. Hose, A. Seckinger, G. Mori, S. Vukicevic, E. A. Cavalcanti-Adam, Copresentation of BMP-6 and RGD ligands enhances cell adhesion and BMP-mediated signaling, Cells 8 (12) (2019) 1646, https://doi.org/10.3390/cells8121646.
[55] P. Roca-Cusachs, N.C. Gauthier, A. Del Rio, M.P. Sheetz, Clustering of alpha(5)beta (1) integrins determines adhesion strength whereas alpha(v)beta(3) and talin enable mechanotransduction, Proc. Natl. Acad. Sci. U.S.A. 106 (38) (2009) 16245–16250, https://doi.org/10.1073/pnas.0902818106.
[56] D. Duan, R. Derynck, Transforming growth factor-beta (TGF-beta)-induced up-regulation of TGF-beta receptors at the cell surface amplifies the TGF-beta response, J. Biol. Chem. 294 (21) (2019) 8490–8504, https://doi.org/10.1074/jbc.RA118.005763.
[57] J.P. Spatz, S. Mössmer, C. Hartmann, M. Möller, T. Herzog, M. Krieger, H.-G. Boyen, P. Ziemann, B. Kabius, Ordered deposition of inorganic clusters from micellar block copolymer films, Langmuir 16 (2) (2000) 407–415, https://doi.org/10.1021/la990070n.
[58] R. Glass, M. Möller, J.P. Spatz, Block copolymer micelle nanolithography, Nanotechnology 14 (10) (2003) 1153.